

REDUCED MULTISCALE COMPUTATION ON ADAPTED GRID FOR THE CONVECTION-DIFFUSION ROBIN PROBLEM*

Shan Jiang^{1,2,†}, Meiling Sun³ and Yin Yang⁴

Abstract We propose a reduced multiscale finite element method for a convection-diffusion problem with a Robin boundary condition. The small perturbed parameter would cause boundary layer oscillations, so we apply several adapted grids to recover this defect. For a Robin boundary relating to derivatives, special interpolating strategies are presented for effective approximation in the FEM and MsFEM schemes, respectively. In the multiscale computation, the multiscale basis functions can capture the local boundary layer oscillation, and with the help of the reduced mapping matrix we may acquire better accuracy and stability with a less computational cost. Numerical experiments are provided to show the convergence and efficiency.

Keywords Multiscale finite element computation, Singular perturbation, Robin problem, Adapted grid, Reduced matrix.

MSC(2010) 35J25, 65N12, 65N30.

1. Introduction

Singularly perturbed problems arise in many scientific fields, such as elastic mechanics, fluid mechanics, molecular dynamics, optimal control, etc. Small singular parameters ε would lead to boundary layer, rapid oscillation or other troublesome behaviors. Traditional numerical methods, such as the finite element method (FEM) or the finite difference method (FDM) is so costly that sufficiently fine discretizations would cause prohibitively challenging systems for solving. Now there is a strong

[†]the corresponding author. Email address: jiangshan.jason@yahoo.com (S. Jiang)

¹School of Science, Nantong University, Nantong 226019, China

²Department of Mathematics, Institute for Scientific Computation, Texas A&M University, College Station, TX 77843, USA

³Department of Public Courses, Nantong Vocational University, Nantong 226007, China

⁴Hunan Key Laboratory for Computation and Simulation in Science and Engineering, Key Laboratory of Intelligent Computing and Information Processing of Ministry of Education, Xiangtan University, Xiangtan 411105, China

*The authors were supported by National Natural Science Foundation of China (11771224 and 11301462), Jiangsu Province Qing Lan Project and Jiangsu Overseas Research Program for University Prominent Teachers to Shan Jiang. And also supported by National Natural Science Foundation of China (11671342 and 91430213), and Hunan Education Department Key Project (17A210) to Yin Yang.

trend in addressing efficient methods for singular perturbations (see [17, 20]).

In decades, multiscale methods are hot spots in recent researches and have a great deal of applications. From a macroscopical point of view, it has an advantage of small computational cost but is hard to reflect the overall microscopic mechanism. On the other hand, from a microscopic point of view, even though it captures tiny process, applying a totally microscopic technology is irrational or even impossible because of computer limitation. In a way, multiscale computations emerge because of a great demand. They are focused on finding a reasonable balance between accuracy and cost, and can be integrated with the singular perturbation (see [14, 15, 18]).

Among these studies, the multiscale finite element method (MsFEM) is one of the popular techniques. It obtains a large scale solution accurately and efficiently by constructing the multiscale basis functions; these bases can be achieved by solving a local problem in coarse elements. E et al. [4] give a systematic review of the heterogeneous multiscale method (HMM), including its designing philosophy and error analysis. In [5] Efendiev, Galvis, and Hou present a generalized multiscale finite element method (GMsFEM), which is to apply the MsFEM with spectral multiscale basis functions by using eigenvectors of local eigenvalue problems, and construct the offline and online spaces for more general problems. An adaptive reduced basis finite element heterogeneous multiscale method (RB-FE-HMM) is provided for elliptic problems with multiple scales in [1], and then an adaptive multiscale finite element method is developed in [7]. In [23] we apply an enriched MsFEM to solve the two dimensional singularly perturbed reaction-diffusion problem, and the multiscale basis functions are combined with a modified version of graded meshes for accuracy and efficiency. Efendiev et al. [6] design a multiscale model reduction framework within the hybridizable discontinuous Galerkin (HDG) finite element method. A residual-driven online generalized multiscale finite element method is studied in [3]. Hou and Liu [8] consider special harmonic multiscale basis functions with an optimal approximation property for fixed local boundary conditions, and achieve proper simulations through the singular value decompositions of some over-sampling operators. Song, Deng, and Wu [22] construct a combined finite element and over-sampling multiscale Petrov-Galerkin method (FE-OMsPGM) to solve the multiscale problems which may have singularities in some special portions, and use much less degree of freedoms than the FEM, which may be more accurate than the OMsPGM. Jiang, Presho, and Huang [13] propose an adapted PG-MsFEM to effectively solve the singularly perturbed reaction-diffusion problem, and reduce the boundary layer errors on the exponential layer adapted meshes; it could eliminate the cell resonance effect automatically to improve the convergence rate. In addition, there are plenty of multiscale and singular perturbation works, such as [11, 16, 19], and so on.

This paper is organized as follows. In Section 2 we introduce a convection-diffusion model with small parameter ε for different boundary conditions, and we build several adapted grids for possible singular boundary layers. In Section 3 we present a multiscale finite element computation with a reduced matrix to solve the perturbed Robin model. In Section 4, boundary approximation strategies are provided for the traditional FEM and the multiscale FEM, respectively. Numerical experiments are presented in Section 5 to demonstrate that the reduced MsFEM on an adapted grid performs well, which ensures accuracy and stability. Finally we conclude in Section 6.

2. Model problem and adapted grid

2.1. Convection-diffusion Robin problem

Consider the one dimensional convection-diffusion model with a Robin boundary condition

$$\begin{cases} Lu := -\varepsilon u''(x) + b(x)u'(x) + c(x)u(x) = f(x), & \text{in } x \in I = (0, 1), \\ k_1 u(0) + k_2 u'(0) = u_L, \quad k_3 u(1) + k_4 u'(1) = u_R, \end{cases} \quad (2.1)$$

where $u(x)$ is the exact solution, $b(x)$ and $c(x)$ are the varying coefficients, $b(x) \geq 2\beta > 0$, and $f(x)$ is the right force. And each constant k_i is zero or non-zero, according to different types of boundary condition. We use ∂I to denote the boundary of the interval I , and $\varepsilon \ll 1$ is a perturbed parameter. It is well-known that small ε will bring the so-called boundary layer phenomena, which makes the traditional methods lose their accuracy and stability.

Lemma 2.1 ([2]). *For $0 \leq k \leq 4$, the k -th order derivative of u has the bound*

$$|u^{(k)}(x)| \leq C(1 + \varepsilon^{-k} e(x, \beta, \varepsilon)),$$

where $e(x, \beta, \varepsilon) = e^{-\frac{\beta x}{\varepsilon}} + e^{-\frac{\beta(1-x)}{\varepsilon}}$. And

$$u(x) = v(x) + w(x)$$

satisfies $Lu = f$, where the smooth part $v(x)$ and the boundary layer part $w(x)$ satisfy $Lv = f$ and $Lw = 0$, and

$$\begin{aligned} |v^{(k)}(x)| &\leq C, \\ |w^{(k)}(x)| &\leq C \cdot \varepsilon^{-k} e(x, \beta, \varepsilon). \end{aligned}$$

The accurate and stable solution of problem (2.1) is our target, and we attempt to pursue a uniformly convergent approximation to the exact solution, which is independent of parameter ε .

The variational form of (2.1) is to seek $u \in H^1$ such that

$$a(u, v) = (f, v), \quad \forall v \in H^1, \quad (2.2)$$

where

$$a(u, v) = \int_0^1 (\varepsilon u'v' + b(x)u'v + c(x)uv) dx, \quad (2.3)$$

$$(f, v) = \int_0^1 f v dx. \quad (2.4)$$

Here $H^1 = \{f | f \in L^2, f' \in L^2\}$ and L^2 is a square integrable space.

The bilinear form $a(\cdot, \cdot)$ is elliptical and continuous,

$$\begin{aligned} C_1 |v|_{1,\Omega}^2 &\leq a(v, v) \leq C_2 |v|_{1,\Omega}^2, & \forall v \in H_0^1(\Omega), \\ |a(u, v)| &\leq C |u|_{1,\Omega} |v|_{1,\Omega}, & \forall u, v \in H_0^1(\Omega). \end{aligned}$$

2.2. Adapted grid partition

Given model (2.1) with a large parameter ε , since traditional methods address well and there is no need for a great number of partition, in a way we use the Uniform grid is enough. However, with a small ε it will produce boundary layers of width $O(\tau) = O(\varepsilon \ln N)$, where N is the partition number. At this time, even though a very huge partition N is used, the traditional method solves the problem invalidly and it may perform a troublesome simulation.

Two typical strategies have been studied for the numerical solution of singularly perturbed partial differential equations. One is the h refinement (h denotes the mesh size) on layer-adapted meshes. The other is the p refinement (p is degree of approximating polynomials), or hp refinement (a combination of h and p refinements), see [9, 10].

We make the a-priori estimation for the problem and know a brief location of boundary layers, and then we may apply a non-Uniform grid partition. Keeping the total partition number unchanged, some subintervals are refined to approximate the boundary layer, while other subintervals are coarsened to approximate the smooth part. This is called the h -mode adapted strategy.

First we use the Shishkin idea to form a block Uniform grid. Then each block is partitioned to equidistant nodes [21]. For example, a transitional point τ is used to divide the interval into two parts: boundary layer subinterval $[0, \tau]$ and smooth one $[\tau, 1]$, both being partitioned by $N/2$ elements. The Shishkin grid node x_i is defined as

$$\text{Shishkin: } x_i = \begin{cases} \frac{2\tau}{N} \cdot (i - 1), & i = 1, \dots, \frac{N}{2} + 1, \\ \tau + \frac{2(1-\tau)}{N} \cdot (i - \frac{N}{2} - 1), & i = \frac{N}{2} + 2, \dots, N + 1. \end{cases} \tag{2.5}$$

The second modification is the Graded grid, which is a highly anisotropic non-Uniform grid, and it can be generated by choosing suitable mesh functions. Making use of a space tensor product, and taking smooth part $[0, 1 - \tau]$ and boundary layer $[1 - \tau, 1]$ for example, the Graded grid node x_i is defined as

$$\text{Graded: } x_i = \begin{cases} \frac{2(1-\tau)}{N} \cdot (i - 1), & i = 1, \dots, \frac{N}{2} + 1, \\ 1 - \tau \left(\frac{2(N+1-i)}{N} \right)^\lambda, & i = \frac{N}{2} + 2, \dots, N + 1, \end{cases} \tag{2.6}$$

where λ is an integer greater than 1.

Furthermore, a Bakhvalov grid is presented to be an adapted layer one, and it should be computed according to boundary layers. Taking a transitional point $\tau = \frac{\varepsilon \ln N}{\beta}$, and suppose that there is two boundary layers with width τ near two ends. Then we divide the interval into three sub-intervals: two boundary layers $[0, \tau]$, $[1 - \tau, 1]$ and one interior smooth $[\tau, 1 - \tau]$. When the boundary layer is near $x = 0$, the node distribution is determined by $e^{-\frac{\beta x_i}{\varepsilon}} = Ai + B$ and $x_1 = 0$, $x_{\frac{N}{4}+1} = \tau$. When the boundary layer is near $x = 1$, its distribution is determined by $e^{-\frac{\beta(1-x_i)}{\varepsilon}} = Ci + D$ and $x_{\frac{3N}{4}+1} = 1 - \tau$, $x_{N+1} = 1$. Then we have

$$A = \frac{4 - 4N}{N^2},$$

$$B = \frac{N^2 + 4N - 4}{N^2},$$

$$C = \frac{4N - 4}{N^2},$$

$$D = \frac{-3N^2 + 4}{N^2}.$$

In this way the Bakhvalov grid node x_i is defined as

$$\text{Bakhvalov: } x_i = \begin{cases} -\varepsilon \ln[1 + \frac{4(1-N)(i-1)}{N^2}], & i = 1, \dots, \frac{N}{4} + 1, \\ \tau + \frac{2(1-2\tau)}{N} \cdot (i - \frac{N}{4} - 1), & i = \frac{N}{4} + 2, \dots, \frac{3N}{4} + 1, \\ 1 + \varepsilon \ln[1 + \frac{4(1-N)(N+1-i)}{N^2}], & i = \frac{3N}{4} + 2, \dots, N + 1. \end{cases} \quad (2.7)$$

In what is mentioned above we provide four kinds of grid partition; they are Uniform, Shishkin, Graded, and Bakhvalov. In the following, we will apply the finite element method and multiscale finite element method, respectively, to solve the singularly perturbed convection-diffusion model on these adapted grids. We are encouraged to verify the simulation superiority of the multiscale computation plus the adapted grid. Note that there is no so-called the most optimal grid for a singular perturbation, and each one should be adjusted to the corresponding situation. Furthermore, we point out that one dimensional node partition may be expanded to higher dimensional problems, which is with a inner product modification of the grid nodes.

3. Finite element and reduced multiscale computation

3.1. Finite element computation

Defining \mathcal{K}^h as a grid partition, we build the standard finite element space

$$V^h = \{v_h \in H^1(I) : v_h|_K \in \mathbb{P}^1(K), \forall K \in \mathcal{K}^h\}, \quad (3.1)$$

where $\mathbb{P}^1(K)$ represents the piecewise linear polynomials in element K . If the Galerkin finite element method is applied, its corresponding variational form is to seek $u_g \in V^h$ such that

$$a(u_g, v) = (f, v), \quad \forall v \in V^h, \quad (3.2)$$

where u_g is the Galerkin FEM solution.

For example, if we use the linear basis function $\psi_1 = 1 - \xi$, $\psi_2 = \xi$, $\xi = \frac{x-x_i}{h}$ being an isoparametric element, then their derivatives $\psi'_1 = -\frac{1}{h}$ and $\psi'_2 = \frac{1}{h}$. According to the variational form (3.2), after using integration by parts, the local stiffness matrix in each element is computed as

$$\begin{aligned} a_{11} &= \int_{x_i}^{x_{i+1}} [\varepsilon \psi'_1 \psi'_1 - (b_1 \psi_1 + b_2 \psi_2) \psi_1 \psi'_1 + (c_1 \psi_1 + c_2 \psi_2) \psi_1 \psi_1] \cdot dx \\ &= \int_0^1 [\frac{\varepsilon}{h^2} - (b_1(1-\xi) + b_2\xi)(1-\xi)(-\frac{1}{h}) + (c_1(1-\xi) + c_2\xi)(1-\xi)^2] \cdot h d\xi \\ &= [\frac{\varepsilon}{h^2} + (\frac{1}{3}b_1 + \frac{1}{6}b_2)\frac{1}{h} + (\frac{1}{4}c_1 + \frac{1}{12}c_2)] \cdot h, \end{aligned}$$

$$\begin{aligned}
a_{12} &= \int_{x_i}^{x_{i+1}} [\varepsilon \psi_1' \psi_2' - (b_1 \psi_1 + b_2 \psi_2) \psi_1 \psi_2' + (c_1 \psi_1 + c_2 \psi_2) \psi_1 \psi_2] \cdot dx \\
&= \left[-\frac{\varepsilon}{h^2} + \left(\frac{1}{6}b_1 + \frac{1}{3}b_2\right)\frac{1}{h} + \left(\frac{1}{12}c_1 + \frac{1}{12}c_2\right) \right] \cdot h, \\
a_{21} &= \int_{x_i}^{x_{i+1}} [\varepsilon \psi_2' \psi_1' - (b_1 \psi_1 + b_2 \psi_2) \psi_2 \psi_1' + (c_1 \psi_1 + c_2 \psi_2) \psi_2 \psi_1] \cdot dx \\
&= \left[-\frac{\varepsilon}{h^2} - \left(\frac{1}{3}b_1 + \frac{1}{6}b_2\right)\frac{1}{h} + \left(\frac{1}{12}c_1 + \frac{1}{12}c_2\right) \right] \cdot h, \\
a_{22} &= \int_{x_i}^{x_{i+1}} [\varepsilon \psi_2' \psi_2' - (b_1 \psi_1 + b_2 \psi_2) \psi_2 \psi_2' + (c_1 \psi_1 + c_2 \psi_2) \psi_2 \psi_2] \cdot dx \\
&= \left[\frac{\varepsilon}{h^2} - \left(\frac{1}{6}b_1 + \frac{1}{3}b_2\right)\frac{1}{h} + \left(\frac{1}{12}c_1 + \frac{1}{4}c_2\right) \right] \cdot h,
\end{aligned}$$

and the local right force vector is

$$\begin{aligned}
F_1 &= \int_{x_i}^{x_{i+1}} f(x) \psi_1 \cdot dx \\
&= \int_{x_i}^{x_{i+1}} (f_1 \psi_1 + f_2 \psi_2) \psi_1 \cdot dx \\
&= \left(\frac{1}{3}f_1 + \frac{1}{6}f_2\right) \cdot h,
\end{aligned}$$

$$\begin{aligned}
F_2 &= \int_{x_i}^{x_{i+1}} f(x) \psi_2 \cdot dx \\
&= \int_{x_i}^{x_{i+1}} (f_1 \psi_1 + f_2 \psi_2) \psi_2 \cdot dx \\
&= \left(\frac{1}{6}f_1 + \frac{1}{3}f_2\right) \cdot h.
\end{aligned}$$

In this way through the nodes data structure, we assemble the global linear algebraic equations $Au = F$ on the fine grid and solve it to obtain the FEM solution.

3.2. Reduced multiscale finite element computation

Being different from the above traditional FEM, the main idea of the multiscale FEM is to capture large scale information by constructing the multiscale basis functions through the finite element scheme, and this can be achieved by solving the basis functions from the local problem, according to the differential operator of the problem. As a result, it costs a low dimensional representation to obtain the large scale solution accurately and efficiently.

We divide the whole interval I into smooth and boundary layer parts with respect to $\tau = \min\{\frac{1}{2}, \frac{\varepsilon \ln N}{\beta}\}$, and the discrete multiscale basis functions are defined on each coarse element $K \in \mathcal{K}^h$. For the MsFEM, its corresponding variational form is to seek $u_h \in U^h$ such that

$$a(u_h, v) = (f, v), \quad \forall v \in U^h, \quad (3.3)$$

where u_h is the MsFEM solution. The multiscale functional space U^h is generated by the multiscale basis functions. In this way the enriched space may reflect the microscopic information of the original problem (2.1).

On each coarse element K we solve the local homogeneous problem for multiscale basis functions

$$\begin{cases} L\varphi_i := -\varepsilon\varphi_i''(x) + b(x)\varphi_i'(x) + c(x)\varphi_i(x) = 0, & \text{in } K, \\ \varphi_i(x_j) = \delta_{ij}, & \text{on } \partial K. \end{cases} \quad (3.4)$$

We refine the Kronecker condition δ_{ij} of this subproblem, that is, $\varphi_i(x_j) = 1$ when $i = j$ and $\varphi_i(x_j) = 0$ when $i \neq j$. Since the local problem (3.4) and the original problem (2.1) have the same differential operator, we apply the FEM to solve (3.4) for the discrete φ_i by using the fine partition M in the coarse element K . As a consequence, the boundary layer microscopic information on the coarse grid with the coarse mesh size H is captured through the multiscale basis φ_i , which is a discrete form and is no of explicit expression like the above linear basis ψ_i . This is quite different from the traditional FEM, who is computed on the fine grid with the fine mesh size h .

The boundary condition of the local problem (3.4) is important to multiscale basis functions, even to the whole original problem. In [12] the authors provide the choosing rule of the linear condition or the oscillatory condition to affect the well-being of ergodicity for some cases. Basically, since our problem is one dimensional case, each coarse element boundary ∂K is made up of two separated nodes, and the boundary condition has no choice but to be unique, which is different for a higher dimensional case. As a result, these multiscale basis functions can reflect the microscopic property of the original problem, such as the boundary layer, scale oscillation, and periodicity.

We construct the multiscale functional space

$$U^h = \text{span}\{\varphi_i, \quad \forall K \in \mathcal{K}^h\}. \quad (3.5)$$

It is enriched with the multiscale basis functions, and these basis functions have the ability to capture the local singular perturbation in boundary layers. In the Matlab code we save the obtained discrete multiscale basis in a mapping matrix R , and then every element in each row and column has local microscopic information in the layers. In a way, we get the reduced scale global matrix $A_{\text{ms}} = R * A * R^T$ and global vector $F_{\text{ms}} = R * F$. Through the multiscale finite element scheme we assemble the global linear equations to solve $A_{\text{ms}}u = F_{\text{ms}}$ on the coarse grid. As a consequence, this reduced multiscale computation just costs a low degree of freedoms to acquire an accurate simulation.

From the literatures we know that the effectiveness of multiscale basis functions is crucial. How to eliminate the ill influence among the scales, and how the multiscale basis carries more integrate information, so that the final simulation is more trustworthy is a concern. Note that the traditional FEM solves on fine grids, while the MsFEM solves on coarse grids. We are inclined to demonstrate that the reduced MsFEM is an optimal method to handle the singular perturbation.

4. Boundary strategy

The boundary condition of the original problem (2.1) may be of Dirichlet type, and also may be of Neumann or Robin type with relationship to derivatives. In this section, we provide the boundary details, and the finite element steps are followed.

After the variational form (3.2), we make the nodes partition on different grids, and use the corresponding connection between the nodes and basis functions. Then the large-scale linear algebraic equations are assembled. For example, the linear basis function is applied as $\psi_i = 1 - \xi$, $\psi_{i+1} = \xi$, where $\xi = \frac{x-x_i}{h_i}$ is a logical element, $h_i = x_{i+1} - x_i$ is a varying mesh size, and $I_i = [x_i, x_{i+1}]$ is a sub-interval. By interpolation we have an approximated solution as

$$\begin{aligned} u_h &= u_i\psi_i + u_{i+1}\psi_{i+1} \\ &= u_i \cdot (1 - \xi) + u_{i+1} \cdot \xi \\ &= u_i \frac{x_{i+1} - x}{x_{i+1} - x_i} + u_{i+1} \frac{x - x_i}{x_{i+1} - x_i}, \quad x \in I_i, \quad i = 1, 2, \dots, N. \end{aligned}$$

For the Dirichlet boundary as $u(0) = u_L$, $u(1) = u_R$, that is,

$$\begin{cases} u_1 = u_L, \\ u_{N+1} = u_R. \end{cases}$$

It is simple to determine the first row and the last row in the global stiffness matrix. Then according to the nodes data we assemble the other rows and form the following linear equations as

$$\begin{pmatrix} 1 & 0 & 0 & \dots & 0 \\ \vdots & \ddots & \ddots & \ddots & \vdots \\ \vdots & \ddots & \ddots & \ddots & \vdots \\ \vdots & \ddots & \ddots & \ddots & \vdots \\ 0 & 0 & \dots & 0 & 1 \end{pmatrix} \begin{pmatrix} u_1 \\ u_2 \\ \vdots \\ u_N \\ u_{N+1} \end{pmatrix} = \begin{pmatrix} u_L \\ \vdots \\ \vdots \\ \vdots \\ u_R \end{pmatrix}. \tag{4.1}$$

When the Neumann boundary with derivatives is considered, we have an approximated derivative as

$$\begin{aligned} u'_h &= u_i\psi'_i + u_{i+1}\psi'_{i+1} \\ &= u_i \frac{-1}{x_{i+1} - x_i} + u_{i+1} \frac{1}{x_{i+1} - x_i}, \quad x \in I_i, \quad i = 1, 2, \dots, N. \end{aligned}$$

The condition $u'(0) = u_L$, $u'(1) = u_R$ means that

$$\begin{cases} u_1 \frac{-1}{h} + u_2 \frac{1}{h} = u_L, \\ u_N \frac{-1}{h} + u_{N+1} \frac{1}{h} = u_R. \end{cases}$$

In this way, the first row and the last row are determined as

$$\begin{pmatrix} \frac{-1}{h} & \frac{1}{h} & 0 & \dots & 0 \\ \vdots & \ddots & \ddots & \ddots & \vdots \\ \vdots & \ddots & \ddots & \ddots & \vdots \\ \vdots & \ddots & \ddots & \ddots & \vdots \\ 0 & 0 & \dots & \frac{-1}{h} & \frac{1}{h} \end{pmatrix} \begin{pmatrix} u_1 \\ u_2 \\ \vdots \\ u_N \\ u_{N+1} \end{pmatrix} = \begin{pmatrix} u_L \\ \vdots \\ \vdots \\ \vdots \\ u_R \end{pmatrix}. \tag{4.2}$$

The Robin boundary condition $u(0) = u_L$ and $u(1) + u'(1) = u_R$ means that

$$\begin{cases} u_1 = u_L, \\ u_N \frac{-1}{h} + u_{N+1} \frac{1+h}{h} = u_R. \end{cases}$$

The first row and the last row are determined similarly, and the linear equations are

$$\begin{pmatrix} 1 & 0 & 0 & \cdots & 0 \\ \vdots & \ddots & \ddots & \ddots & \vdots \\ \vdots & \ddots & \ddots & \ddots & \vdots \\ \vdots & \ddots & \ddots & \ddots & \vdots \\ 0 & 0 & \cdots & \frac{-1}{h} & \frac{1+h}{h} \end{pmatrix} \begin{pmatrix} u_1 \\ u_2 \\ \vdots \\ u_N \\ u_{N+1} \end{pmatrix} = \begin{pmatrix} u_L \\ \vdots \\ \vdots \\ \vdots \\ u_R \end{pmatrix}. \quad (4.3)$$

As a consequence, we solve it to get the numerical solution.

It should be noted that the above fine size h could be changed to the coarse size H , if it is used in the multiscale computation, and both could be non-equidistant size h_i or $H_i (= x_{i+1} - x_i)$, depending on what kind of adapted grid (2.5)-(2.7) is used. When we apply the FEM with a very fine grid size h to obtain the FEM solution, the system $Au = F$ of the global linear equations is large-scaled, which is computational cost level of $O(NM)$. However, if we apply the MsFEM with a relative coarse grid size H to obtain the MsFEM solution for enough accuracy, the corresponding equations turn to $A_{ms}u = F_{ms}$ which are relative small-scaled of computational cost $O(N)$, and this shows the superiority of the reduced MsFEM, especially for high dimensional cases.

What is more interesting if high dimensional models are encountered, the above strategy we can extend too. We just need to mark all of the boundary nodes as for specific serial u_i , then modify the concrete lows in the global stiffness matrix A , which is according to corresponding boundary conditions.

5. Numerical experiments

To demonstrate the performance of different methods, we define the finite element method on Uniform grid as FEM(U), on Shishkin grid as FEM(S), on Graded grid as FEM(G), and on Bakhvalov grid as FEM(B), and define the multiscale finite element method on Uniform grid as MsFEM(U), on Shishkin grid as MsFEM(S), on Graded grid as MsFEM(G), and on Bakhvalov grid as MsFEM(B) to solve the convection-diffusion problem, respectively. Still we set N as the coarse element partition number, and M as the fine partition number on each coarse element. Then the FEM solves the problem on a very fine grid NM , while the MsFEM solves it on a relative coarse grid N . With the mesh refinement, we compare the differences among them about the numerical accuracy and stability. And we try to verify that the reduced MsFEM may acquire the uniform-convergence, which is independent of the singular parameter ε .

We define the errors E of L^2 norm and H^1 norm as

$$\|E\|_{L^2} = \left(\int_0^1 (u - u_{\text{approx}})^2 dx \right)^{\frac{1}{2}}, \quad (5.1)$$

$$\|E\|_{H^1} = \left(\int_0^1 (u' - u'_{\text{approx}})^2 dx \right)^{\frac{1}{2}}, \tag{5.2}$$

where u is the exact solution, u_{approx} is the corresponding numerical solution, and their norm is a criterion to judge the advantage of methods.

Example 5.1. Given the exact solution of (2.1)

$$u(x) = \frac{e^{\frac{x-1}{\varepsilon}} - e^{-\frac{1}{\varepsilon}}}{1 - e^{-\frac{1}{\varepsilon}}} + x^2,$$

with the Dirichlet boundary condition $u(0) = 0, u(1) = 2$, we know the boundary layer is near $x = 1$. Setting the non-constant coefficient $b(x) = 1$ and $c(x) = x$, and the right force $f(x) = 2x - 2\varepsilon + xu$. Exact $u(x)$ is shown in Fig. 1, and we find that when $\varepsilon = 10^{-4}$ it will come up with the singularly perturbed boundary layers, which changes rapidly near the boundary and its derivative is huge.

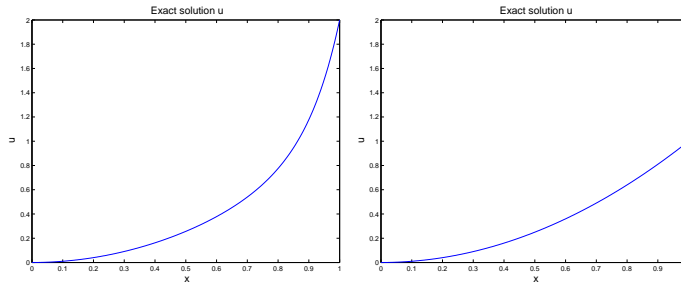


Figure 1. Example 5.1’s exact solution u when $\varepsilon = 10^{-1}, 10^{-4}$, respectively.

Table 1. When $\varepsilon = 10^{-1}$, the L^2 norm errors of FEM(U), FEM(S), FEM(G) and MsFEM(U), MsFEM(S), MsFEM(G).

NM	FEM(U)	FEM(S)	FEM(G)	N	MsFEM(U)	MsFEM(S)	MsFEM(G)
16	3.726e-3	9.257e-4	6.710e-4	4	4.854e-3	2.110e-2	1.192e-2
32	9.544e-4	4.505e-4	1.964e-4	8	1.781e-3	1.620e-3	5.095e-4
64	2.401e-4	1.694e-4	5.182e-5	16	4.825e-4	2.093e-5	1.012e-4
128	6.011e-5	5.695e-5	1.278e-5	32	1.231e-4	4.342e-5	6.417e-5
256	1.503e-5	1.799e-5	2.979e-6	64	3.096e-5	2.041e-5	2.280e-5
512	3.759e-6	5.460e-6	6.508e-7	128	7.754e-6	7.309e-6	6.094e-6
1024	9.397e-7	1.612e-6	1.269e-7	256	1.940e-6	2.324e-6	1.152e-6
2048	2.349e-7	4.658e-7	1.770e-8	512	4.851e-7	6.816e-7	4.600e-8

From Fig. 1a and Table 1 we find that there are no boundary layers for a larger $\varepsilon = 10^{-1}$, and the traditional FEM can solve the problem effectively and its result is the most accurate on the fine Graded grid. At the meantime, the MsFEM performs also well on the relative coarse grid that only costs less computational resources, and it provides a speeding-up convergence finally. To be more specific and fair, the FEM on $NM = 2048$ and the MsFEM on $N = 512$ get the same level accuracy, while the computation for the latter is easier and more relaxed, and has a great advantage in higher dimensions. From Fig. 2 it testifies that the exact solution, the FEM solution, and the MsFEM solution are almost identical when ε is large, and both methods simulate the problem well.

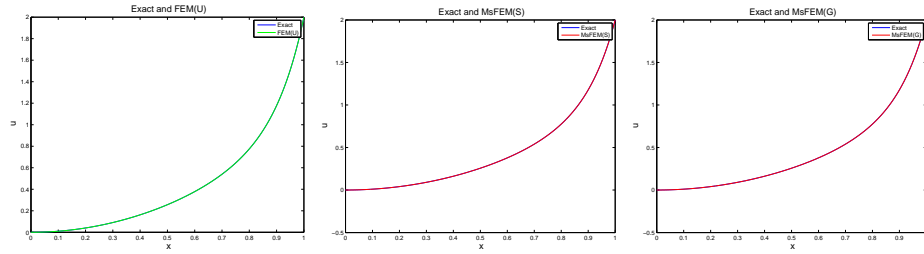


Figure 2. When $\varepsilon = 10^{-1}$, the comparison of exact solution between FEM(U) on $NM = 2048$ or MsFEM(S), MsFEM(G) on $N = 512$.

Table 2. When $\varepsilon = 10^{-4}$, the L^2 norm errors of FEM(U), FEM(S), FEM(G) and MsFEM(U), MsFEM(S), MsFEM(G).

NM	FEM(U)	FEM(S)	FEM(G)	N	MsFEM(U)	MsFEM(S)	MsFEM(G)
32	3.664e-1	9.635e-3	4.972e-3	8	4.244e+0	8.386e-2	1.775e-1
64	1.953e-2	3.727e-3	1.955e-3	16	5.395e-1	1.120e-1	2.067e-2
128	1.452e-2	5.803e-4	3.135e-4	32	1.151e-1	2.136e-1	6.518e-2
256	1.466e-3	1.165e-5	8.570e-6	64	3.401e-2	3.941e-2	7.923e-3
512	8.510e-4	3.061e-6	1.876e-6	128	7.975e-3	3.976e-3	1.106e-3
1024	7.293e-4	9.281e-7	1.911e-6	256	1.757e-3	6.768e-4	4.505e-4
2048	3.463e-4	2.723e-7	2.089e-5	512	4.987e-4	1.705e-4	1.316e-4
4096	—	—	—	1024	2.320e-4	5.809e-5	4.359e-5

From Fig. 1b and Table 2 we find that when $\varepsilon = 10^{-4}$ is smaller, it will bring singular boundary layers. And even worse, the FEM on a very fine grid it can not be computed, and on the Graded grid shows the divergence with the mesh refinement. On the contrary, the MsFEM on a relative coarse grid solves the problem with only a low degree of freedoms to obtain accurate results, and ensures the uniform convergence with the mesh-refinement. From Fig. 3 we observe that the comparison of the FEM(U) with the exact solution is alike in the smooth part, but is far way from each other in the boundary layer part even on a very fine grid $NM = 2048$. However, the MsFEM and the exact solution are almost totally coincident on the relative coarse grid $N = 512$, so its simulation is perfect to a certain extent.

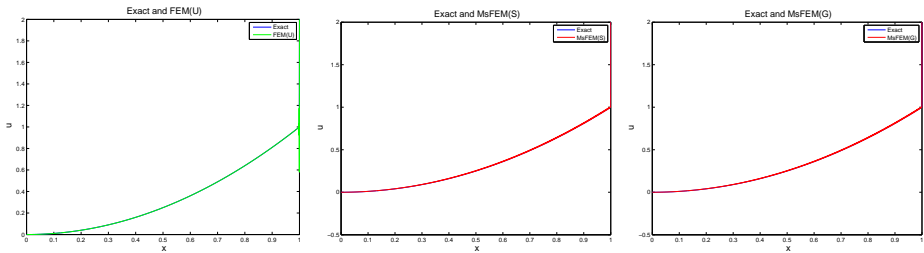


Figure 3. When $\varepsilon = 10^{-4}$, the comparison of exact solution between FEM(U) on $NM = 2048$ or MsFEM(S), MsFEM(G) on $N = 512$.

Example 5.2. Given (2.1) the Robin problem's exact solution

$$u(x) = \frac{e^{m_1 x} - e^{m_2 x}}{(1 + m_1)e^{m_1} - (1 + m_2)e^{m_2}},$$

where $m_1 = \frac{-1 + \sqrt{1 + 4\varepsilon}}{2\varepsilon}$ and $m_2 = \frac{-1 - \sqrt{1 + 4\varepsilon}}{2\varepsilon}$, and setting the Robin boundary condition $u(0) = 0$, $u(1) + u'(1) = 1$. Taking the coefficients $b(x) = -1$ and $c(x) = 1$, and the right force $f(x) = 0$. The exact solution $u(x)$ is shown in Fig. 4, and a small $\varepsilon = 10^{-4}$ may bring the boundary layer near $x = 0$, which gives trouble in numerical simulations.

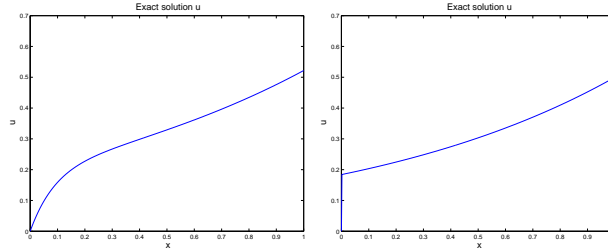


Figure 4. Example 5.2's exact solution u when $\varepsilon = 10^{-1}, 10^{-4}$, respectively.

Table 3. When $\varepsilon = 10^{-4}$, the H^1 norm errors of FEM(U), FEM(S), FEM(B) and MsFEM(U), MsFEM(S), MsFEM(B).

NM	FEM(U)	FEM(S)	FEM(B)	N	MsFEM(U)	MsFEM(S)	MsFEM(B)
16	1.793e-1	4.989e-2	6.804e-3	4	1.863e-1	4.287e-2	3.193e-2
32	2.394e-1	4.038e-2	3.348e-3	8	1.224e-1	1.919e-2	1.568e-2
64	1.679e-1	2.736e-2	1.736e-3	16	4.634e-2	8.465e-3	7.842e-3
128	3.439e-2	7.935e-3	9.475e-4	32	1.792e-2	3.800e-3	3.978e-3
256	4.425e-3	5.554e-4	4.905e-4	64	5.399e-3	2.041e-3	2.059e-3
512	1.178e-3	2.531e-4	2.451e-4	128	1.661e-3	1.064e-3	1.101e-3
1024	3.215e-4	1.268e-4	1.225e-4	256	5.623e-4	5.746e-4	6.291e-4
2048	9.120e-5	6.350e-5	6.125e-5	512	2.116e-4	3.332e-4	4.017e-4
4096	—	—	—	1024	8.894e-5	2.166e-4	2.967e-4

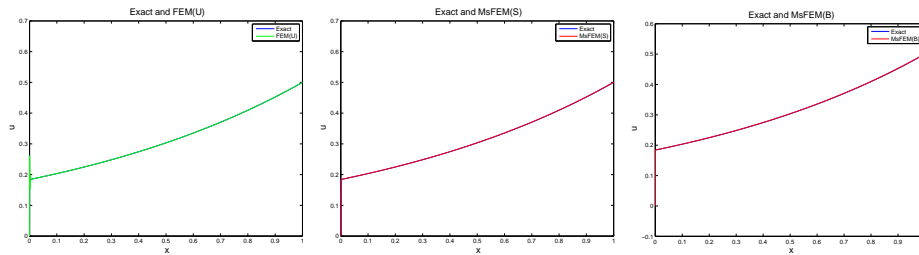


Figure 5. When $\varepsilon = 10^{-4}$, the comparison of exact solution between FEM(U) on $NM = 2048$ or MsFEM(S), MsFEM(B) on $N = 512$.

From Fig. 4b and Table 3 we observe that a small $\varepsilon = 10^{-4}$ will cause the singular boundary layer, and the FEM performs laboriously on fine grids and doesn't

converge on the Graded grid (not being listed here). However, the MsFEM computes on the coarse grid and keeps a uniform-convergence with the mesh refinement. And it is proved the first order H^1 norm convergence, which is in accordance with the mathematical theory. From Fig. 5, when ε is small, even though on a very fine grid $NM = 2048$ the FEM(U) is far away from the exact solution near the boundary $x = 0$. On the other side, the MsFEM on the coarse grid $N = 512$ is almost identical to the exact solution.

Through the numerical experiments we show that, the reduced multiscale finite element computation plus adapted grids can solve the convection-diffusion model with different boundary conditions efficiently. It acquires high accuracy and convergent result, which is independent of the singular parameter ε . This is attributed to the fact that the multiscale basis functions capture the local perturbation. With the help of the adapted grid resulting in the reduced computational cost, the new method simulates the singular perturbation problem excellently.

6. Concluding remarks

In this paper, we present a reduced multiscale computation for a singularly perturbed convection-diffusion model. For different types of boundary conditions such as the Robin type, we apply three interpolating strategies for accurate boundary approximations. As for the possible boundary layer phenomena, several adapted grids are constructed to recover the rapid oscillation. In our multiscale computation, the multiscale basis functions have the ability to capture the local microscopic information. With the help of reduced mapping matrix we just compute on the coarse grids with small computational cost to obtain the accurate and convergent numerical results, which are independent of the singular parameter.

Acknowledgements

We would like to thank the referees and editors for their insightful comments and helpful suggestions, which led to an improvement of the paper.

References

- [1] A. Abdulle and Y. Bai, *Adaptive reduced basis finite element heterogeneous multiscale method*, Comput. Methods Appl. Mech. Engrg., 2013, 257, 203–220.
- [2] X. Cai, D. L. Cai, R. Q. Wu and K. H. Xie, *High accuracy non-equidistant method for singular perturbation reaction-diffusion problem*, Appl. Math. Mech., 2009, 30(2), 175–182.
- [3] E. T. Chung, Y. Efendiev and W. T. Leung, *Residual-driven online generalized multiscale finite element methods*, J. Comput. Phys., 2015, 302, 176–190.
- [4] W. N. E, B. Engquist, X. T. Li, W. Ren and E. Vanden-Eijnden, *Heterogeneous multiscale methods: A review*, Commun. Comput. Phys., 2007, 2(3), 367–450.
- [5] Y. Efendiev, J. Galvis and T. Y. Hou, *Generalized multiscale finite element methods (GMsFEM)*, J. Comput. Phys., 2013, 251, 116–135.

-
- [6] Y. Efendiev, R. Lazarov, M. Moon and K. Shi, *A spectral multiscale hybridizable discontinuous Galerkin method for second order elliptic problems*, *Comput. Methods Appl. Mech. Engrg.*, 2015, 292, 243–256.
- [7] P. Henning, M. Ohlberger and B. Schweizer, *An adaptive multiscale finite element method*, *Multiscale Model. Simul.*, 2014, 12, 1078–1107.
- [8] T. Y. Hou and P. F. Liu, *Optimal local multi-scale basis functions for linear elliptic equations with rough coefficients*, *Discrete Contin. Dynam. Sys. A*, 2016, 36(8), 4451–4476.
- [9] Y. Q. Huang, K. Jiang and N. Y. Yi, *Some weighted averaging methods for gradient recovery*, *Adv. Appl. Math. Mech.*, 2012, 4(2), 131–155.
- [10] Y. Q. Huang, Y. F. Su, H. Y. Wei and N. Y. Yi, *Anisotropic mesh generation methods based on ACVT and natural metric for anisotropic elliptic equation*, *Science China: Mathematics*, 2013, 56(12), 2615–2630.
- [11] L. J. Jiang and Q. Q. Li, *Reduced multiscale finite element basis methods for elliptic PDEs with parameterized inputs*, *J. Comput. Appl. Math.*, 2016, 301, 101–120.
- [12] S. Jiang and Y. Q. Huang, *Numerical investigation on the boundary conditions for the multiscale base functions*, *Commun. Comput. Phys.*, 2009, 5(5), 928–941.
- [13] S. Jiang, M. Presho and Y. Q. Huang, *An adapted Petrov-Galerkin multiscale finite element for singularly perturbed reaction-diffusion problems*, *Inter. J. Comput. Math.*, 2016, 93(7), 1200–1211.
- [14] J. Kevorkian, and J. D. Cole, *Multiple Scale and Singular Perturbation Methods*, Springer-Verlag, New York, 1996.
- [15] R. C. Lin and M. Stynes, *A balanced finite element method for singularly perturbed reaction-diffusion problems*, *SIAM J. Numer. Anal.*, 2012, 50(5), 2729–2743.
- [16] N. Madden and S. Russell, *A multiscale sparse grid finite element method for a two-dimensional singularly perturbed reaction-diffusion problem*, *Adv. Comput. Math.*, 2015, 41, 987–1014.
- [17] J. J. Miller, E. O’Riordan and G. I. Shishkin, *Fitted Numerical Methods for Singular Perturbation Problems (revised edition)*, World Scientific, Singapore, 2012.
- [18] A. Muntean and M. N. Radu, *A multiscale Galerkin approach for a class of nonlinear coupled reaction-diffusion systems in complex media*, *J. Math. Anal. Appl.*, 2010, 371(2), 705–718.
- [19] M. Presho and J. Galvis, *A mass conservative generalized multiscale finite element method applied to two-phase flow in heterogeneous porous media*, *J. Comput. Appl. Math.*, 2016, 296, 376–388.
- [20] K. Sharma, P. Rai and K. C. Patidar, *A review on singularly perturbed differential equations with turning points and interior layers*, *Appl. Math. Comput.*, 2013, 219(22), 10575–10609.
- [21] G. I. Shishkin, *A finite difference scheme on a priori adapted meshes for a singularly perturbed parabolic convection-diffusion equation*, *Numer. Math. Theor. Meth. Appl.*, 2008, 1(2), 214–234.

-
- [22] F. Song, W. B. Deng and H. J. Wu, *A combined finite element and oversampling multiscale Petrov-Galerkin method for the multiscale elliptic problems with singularities*, J. Comput. Phys., 2016, 305, 722–743.
- [23] M. L. Sun and S. Jiang, *Multiscale basis functions for singular perturbation on adaptively graded meshes*, Advan. Appl. Math. Mech., 2014, 6(5), 604–614.